3-1-2018

Model-Assisted Approach for Probability of Detection (POD) in High-Temperature Ultrasonic NDE Using Low-Temperature Signals

Prathamesh N. Bilgunde
Iowa State University, pratham@iastate.edu

Leonard J. Bond
Iowa State University, bondlj@iastate.edu

Model-Assisted Approach for Probability of Detection (POD) in High-Temperature Ultrasonic NDE Using Low-Temperature Signals

Abstract
Advanced piezoelectric-based ultrasonic transducers offer the potential for in-coolant nondestructive testing (NDT) measurements at high temperatures (HTs), including during hot standby (~260°C) for liquid-sodium–cooled advanced small modular reactors. The reliability of the NDT measurements is typically quantified by the probability of detection (POD) measured at the corresponding temperature. Obtaining such data in liquid sodium is challenging. Using a model-assisted POD approach, a transfer function is reported that enables data obtained on low carbon steel specimens at room temperature to give an estimated POD at an HT. A primary source of the difference in POD between room temperature and HT is due to the transducer material temperature-dependent performance. This paper demonstrates the transfer function approach using data for modified lead zirconium titanate (PZT-5A). A physics-based model was developed using a finite element method and used to quantify reduction in the scattering amplitude for standard reflectors, side drilled holes (SDHs), for a range of sizes, from 15°C to 195°C. Scattering amplitudes for the room-temperature–simulated data are compared with the experimental data measured at 2.25 MHz. A temperature correction and transfer functions were developed to transform the simulated temperature effect in the physics-based model to compare with the experimental data. The model-based approach was validated with experimental data. It was seen and validated for a PZT-5A ultrasonic transducer operating at 2.25 MHz that the 95% POD at 15°C was 0.58 λ, and due to variation in temperature-dependent properties of PZT-5A, the 95% POD was achieved only for a 1.41 λ SDH diameter.

Keywords
MAPOD, high temperature, piezoelectric transducer

Comments
This is the Submitted Manuscript of an article published by Taylor & Francis as Bilgunde, Prathamesh N. and Leonard Bond. "Model-Assisted Approach for Probability of Detection (POD) in High-Temperature Ultrasonic NDE Using Low-Temperature Signals." *Nuclear Technology*, 2018. Available online. DOI: 10.1080/00295450.2017.1419782. Posted with permission.

Model Assisted approach for Probability of Detection (POD) in High Temperature Ultrasonic NDE using Low Temperature Signals

Prathamesh N. Bilgunde and Leonard J. Bond

Department of Aerospace Engineering and Center for Nondestructive Evaluation (CNDE)

Iowa State University, Ames, IA 50011

Email: pratham@iastate.edu

Number of pages: 25

Number of figures: 10

Number of tables: 3

Abstract

Advanced piezoelectric based ultrasonic transducers offer the potential for in-coolant NDT measurements at high temperatures, including during hot stand-by (~260C) for liquid sodium cooled advanced small modular reactors (SMRs). The reliability of the NDT measurements is typically quantified by the probability of detection (POD) measured at the corresponding temperature. Obtaining such data in liquid sodium is challenging. Using a model assisted probability of detection (MAPOD) approach a transfer function is reported that enables data obtained on low carbon steel specimens at room temperature to give an estimated POD at higher temperature. A primary source of the difference in POD between room and high temperature is due to the transducer material temperature dependent performance. This paper demonstrates the transfer function approach using data for modified lead zirconium titanate (PZT-5A). A physics based model was developed using a finite element method and used to quantify reduction in the scattering amplitude for standard reflectors, side drilled holes (SDH), for a range of sizes, from 15 to 195C. Scattering amplitudes for the room temperature simulated data is compared with the experimental data measured at 2.25 MHz. A temperature correction and transfer functions were developed to transform the simulated temperature effect in the physics based model to compare with the experimental data. The model based approach was validated with experimental data. It was seen and validated for a PZT-5A ultrasonic transducer operating at 2.25MHz that the 95% POD at 15C was 0.58λ and due to variation in temperature dependent properties of PZT-5A, the 95% POD was only achieved for a 1.41 λ SDH diameter.

Keywords: MAPOD, high temperature, piezoelectric transducer

I. Introduction

Generation IV fast nuclear reactor designs are being developed to support sustainable development, economic competitiveness, and improved safety [1]. Past experience, specifically, with regard to long term maintenance experience from the Phoenix reactors (France) has underlined the need to provide effective and reliable inspection of components [2]. The efficacy of the NDT inspection is often quantified by the probability of detection (POD) curve. Previous studies have shown that signal to noise ratio becomes a critical issue for transducers operating in liquid sodium at a hot stand-by temperature of 260C [3]. Particularly, the reduction in the signal strength as a function of temperature reduces the ability to identify and distinguish between an ultrasonic response from the defect and electrical noise. This reduction in signal strength can cause a reduction in POD in a high temperature (HT) environment that needs to be predicted. From POD perspective, actual non-destructive inspection is highly variable due to human factors, experimental limitations etc. Moreover, these experiments are time consuming and expensive due to the cost of the preparation of specimens with defects. A more cost-effective approach to increase confidence is using physics based modeling to predict POD, and this has been demonstrated for many years [4]. Sarkar et al. [5] proposed a modeling methodology to estimate POD as a function of known fixed effect parameters. These models have been an integral part of a unified approach for model assisted probability of detection (MAPOD) [6-7]. The basic idea behind MAPOD is to use an understanding of the effects of physical factors on the measurement results [6]. Cobb et al. [8] advocated development of hybrid finite element models to use in the MAPOD approach. The thesis of this work states that predictive modeling should be multi-domain consisting of sensor, electronics, and power management. Crack geometry was the primary source of variability in this work [8]. Smith et al. developed the Full Model-Assisted (FMAPOD) approach [9] and also presented a transfer function approach [10] that correlated the responses from an artificial defect to that of a real crack geometry. Aldrin et al. [11] reported simulation-based POD studies for reliability assessment of structural health monitoring (SHM) systems within the framework of MAPOD. Jensen et al. [12] explored uncertainty propagation through CIVA-multi technique software (CEA-LIST, France)

simulation models. Wirdelius et al. [13] also developed POD based on synthetic data obtained from simSUNDT software. Pavlovi et al. [14] reported POD data as a function of multiple parameters in contrast to the conventional signal response analysis. Li et. al. [15] developed a statistical model for estimating POD based on the physical mechanisms of ultrasonic inspection. This work [15] successfully demonstrates the intersection of statistical and physical modeling of ultrasonic wave propagation for the purpose of estimating POD.

In a harsh operating environment, such as a nuclear reactor, POD can be expected to reduce over time due to deterioration of sensor performance. Subair et al. [16] reported finite element modeling for the estimation of POD of nuclear components at room temperature. Roy et al. [17] developed temperature dependent, physics based modeling using experimental data up to 80C. The objective of this work [17] was to propose a temperature compensation strategy for guided waves. Similarly, Wang et al. [18] reported an adaptive filtering technique for temperature compensation of Lamb waves. Recently, Salmanpour et al. [19] proposed a new method of temperature correction and used it in conjunction with a delay and sum damage detection algorithm. The proposed method is based on baseline signal stretch with an improved minimum residual allowing correction over a larger temperature range. Gianneo et al. [20] reported the FMAPOD approach for inspection of a copper canister to plot the POD curve for flat bottom holes (FBH) where data were calculated using CIVA-multi technique software (CEA-LIST, France). In this work, the primary source of variability was structural attenuation. Gianneo [21] extended this work using finite element models for a multi-parameter POD formulation for a Lamb waves–based SHM for light alloy aeronautical plates. Yusa et al. [22] evaluated general effects of flaw parameters on the ultrasonic response using the numerical simulations and experimental measurements on 316L steel specimens. Recently, Janapati et al. [23] discussed role of POD in NDE and SHM. The focus of this work was quantifying the effect of transducer parameters on damage detection sensitivity.

However, the effect of temperature dependency of piezoelectric material on the POD is not sufficiently quantified. In the current work, temperature dependency of PZT-5A is modelled with regards to its effect on the POD. The objective of this work is to connect a microscopic material phenomenon that occurs within

piezoelectric ceramics at a high temperature to an industrial practice of evaluating POD for quantifying performance of NDT inspections. This is achieved by a physics based model using finite element (FE) software COMSOL™ (Burlington, MA) [24] and temperature dependent material coefficients of PZT-5A [25]. Using the FE model, temperature correction and transfer factors are proposed to estimate POD value at high temperature using POD of room temperature experimental data.

II. Problem Description

The problem considered in this work consists of a planar compression wave (P-wave) transducer transmitting at normal incidence through a solid-solid interface as shown in Fig.1. Let Ω be the domain of the problem connected by the Lipschitz boundaries $\partial\Omega$ .The low carbon steel block of 50mm x 50mm cross section and the piezoelectric transducer are represented by domain Ω_{steel} and $\Omega_{transducer}$ respectively. The piezoelectric material PZT-5A domain has a length of 12.7 mm and a thickness of 0.9 mm. Hence, the computational domain is given by $\Omega = \Omega_{Steel} \cup \Omega_{transducer}$ as shown in Fig.1.

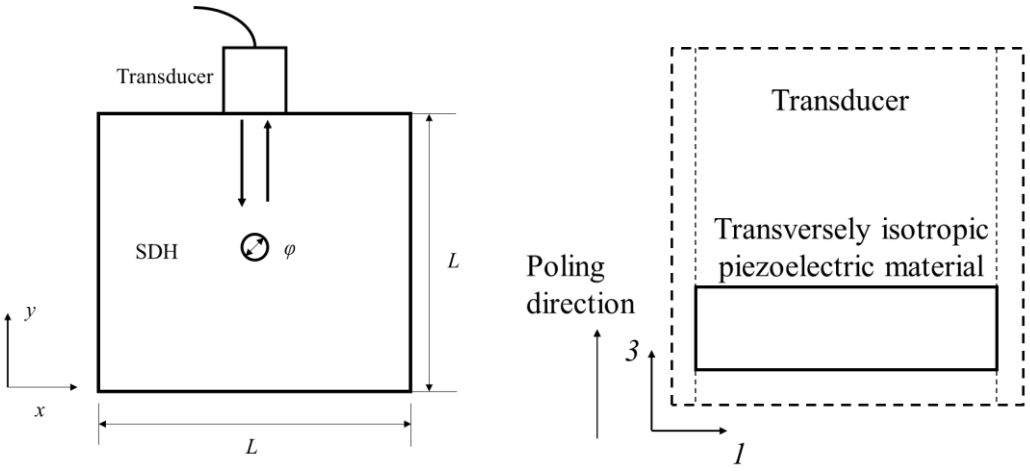

Fig. 1 Problem configuration to predict the response from SDHs at normal incidence

The elastic wave is scattered by the side drilled hole (SDH) in the solid. The P-wave response from the SDH is received by the same transducer in a pulse-echo solid-solid interface model. It is assumed that the plane of transducer is perpendicular to the axis of the SDH. In the current work, amplitude of planar compression wave (P-wave) reflected from SDHs is computed in terms of the vertical component of the

displacement field in the finite element model. The assumptions for the physics based model are summarized are given as:

(a) plain strain condition (b) the material behaves linearly elastic (c) small deformation of the plate, which thus implies that this theory is not applicable for large deformations of the piezoelectric material. This assumption is particularly valid for the low-power piezoelectric based ultrasonic transducers which are used in linear ultrasonic measurements employed in SHM and NDE. (d) Material is continuous and homogenous which assumes uniform distribution of material properties to solve the problem within a continuum mechanics framework. This prevents the current approach from applying to the materials with significant discontinuity and inhomogeneity. (e) Damping variation due to temperature is assumed negligible since the objective of the current work is to primarily study effect of temperature dependent piezoelectric material properties as a function of temperature. Damping mainly causes changes in the magnitude and bandwidth of the resonance frequency response. Hence, if the Rayleigh damping coefficients as a function of temperature are measured, the temperature dependent damping response can be included in the current transient FE model. The pyroelectric and magnetization effect contribute to the mechanical strain and electric displacement of the piezoelectric material as shown in equations (1-2). (f) However, the thermoelectric coupling resulting in a pyroelectric effect in the piezoelectric material is not considered and (g) magnetization effect are assumed negligible, reasons of which are discussed in the next section.

III. Physics based model

III.A Constitutive equation of piezoelectric material for temperature dependence

The equations for piezoelectricity can be obtained using Gibbs thermodynamic potential which is given as [26]

$$S_i = s_{ij}^{E,H,\theta} T_j + d_{mi}^{H,\theta} E_m + d_{mi}^{H,\theta} H_m + \alpha_i^{E,H} d\theta \tag{1}$$

$$D_m = d_{mi}^{H,\theta} T_i + \varepsilon_{mk}^{T,H,\theta} E_k + m_{mk}^{T,\theta} H_k + p_m^{T,H} d\theta \tag{2}$$

where S_i is the Cauchy's total mechanical strain tensor, D is the electric displacement tensor, ε_{mk}^{T} is the absolute permittivity at constant mechanical stress T_i , $s_{ij}^{E,H,\theta}$ is the elastic compliance coefficient at a constant electric field E, constant magnetic field H and constant temperature θ and d_{mi} is the piezoelectric charge coefficient. The thermal expansion coefficient and pyroelectric constant are given by α and p respectively. The magneto-dielectric coefficient is given by m. Phase velocity of elastic waves for piezoelectric ceramic is significantly less than the electromagnetic waves. This implies time derivative of magnetic field $H \approx 0$ indicating absence of magnetization effect and presence of a quasi-static field. Thus magneto-dielectric coupling from (1-2) can be ignored. In the current work, the temperature difference $d\theta$ is assumed to be small representing a gradual increase in the temperature of a piezoelectric based sensor. Thus, for a quasi-thermal change in the piezoelectric material, the thermal expansion and pyroelectric effect can be ignored. This reduces (1-2) to a strain charge form of linear theory of the piezoelectric effect can be given by

$$S_i = s_{ij}^{E} T_j + d_{mi} E_m \tag{3}$$

$$D_m = d_{mi} T_i + \varepsilon_{mk}^{T} E_k \tag{4}$$

The piezoelectric material modeled in this study, PZT 5A, exhibits a crystal structure with a symmetry of a hexagonal 6mm class [25]. The piezoelectric material is considered transversely isotropic if the poling axis aligns with one of the material symmetry axes [25] as shown in the expanded view of transducer model in Fig.1. Hence, for a 2-D physics based model, the material matrix reduces to 4 elastic coefficients, 3 piezoelectric coefficients and 2 dielectric coefficients. Hence the piezoelectric stiffness matrix can be given as

$$S = \begin{bmatrix} s_{11} & s_{13} & 0 & 0 & d_{31} \\ s_{13} & s_{33} & 0 & 0 & d_{33} \\ 0 & 0 & s_{44} & d_{15} & 0 \\ 0 & 0 & d_{15} & \varepsilon_{11} & 0 \\ d_{31} & d_{33} & 0 & 0 & \varepsilon_{33} \end{bmatrix} \tag{5}$$

Further information regarding the temperature dependence of a piezoelectric material is given by Sabat et al. [25]. In the current FE model, the in-plane deformation problem is considered in the x-y plane as shown in Fig.1. Poling axis of the soft PZT-5A coincides with the y-axis of the model. Assumed electromechanical load for the in-plane problem is given by: a) $E_1 \neq 0,\ E_3 \neq 0,\ E_2 = 0$, also implies $D_1 \neq 0,\ D_3 \neq 0,\ D_2 = 0$ *b*) mechanical displacement $u_1 \neq 0,\ u_3 \neq 0,\ u_2 = 0$. Thus, the non-zero stress and strain components are given by $\sigma_{11},\ \sigma_{33},\ \sigma_{13}$ and $s_{11},\ s_{13},\ s_{33}$. The assumption (b) of non-zero mechanical displacement, strain, and stress also applies to linear elastic solids in the physics based model.

III.B Constitutive equations of piezoelectric material for temperature dependence

The equation of linear momentum balance in the time domain is given by [27]

$$\rho \frac{\partial^2 u}{\partial t^2} = \nabla . \sigma + F_v \tag{6}$$

where ρ is the assigned material density, u is the mechanical displacement, σ is second order Piola-Kirchoff stress tensor, and F_v is the body force. The top boundary (y=L) for the Ω_{steel} shown in Fig. 1 is kept traction free ($\sigma_{31} = \sigma_{33} = \sigma_{11} = 0$). A low reflection boundary condition is applied to the Ω_{steel} at x=0 and x=L boundaries to reduce reflection of the wave from side walls which also reduce the degree of freedom for which the model is solved, is given by [24]:

$$\sigma \cdot n = -pC_p \left(\frac{\partial u}{\partial t} \cdot n \right) - pC_s \left(\frac{\partial u}{\partial t} \cdot t \right) t \tag{7}$$

The vertices x=0 and x=L on the bottom boundary (y=0) of the Ω_{steel} are modelled as fixed constraints (u=0) representing the fixed support used to ensure flatness of the structure during ultrasonic contact measurements. The boundaries of SDH are traction free ($\sigma_{31} = \sigma_{33} = \sigma_{11} = 0$).

III.C Electrostatic model for piezoceramic

As previously stated, for the piezoelectric media, the electric field (piezoelectric media) is assumed to be irrotational. Thus, the electric field E is related to the scalar electric potential V by [24]:

$$E = -\nabla V \tag{8}$$

$$n \bullet D = 0 \tag{9}$$

Terminal boundary is assigned to the top electrode of the piezoelectric material which is coupled to the lumped parametric model discussed in the next section. The bottom boundary of the Ω_{PZT} is grounded (V=0). Zero charge constraint is assigned in the domain Ω_{PZT} at boundaries without terminal or ground boundaries given by equation (9). Charge density ρ_v in the domain Ω_{PZT} is given by [24]

$$\nabla \bullet D = \rho_v \tag{10}$$

III.D Excitation of transducer using the lumped parametric circuit model

In the experimental measurements, the piezoelectric transducer is excited with the pulsar-receiver circuit. This introduces electrical impedance mismatch between the transducer and the instrumentation. This can be modelled in a finite element model by introducing a resistor of impedance equal to that of pulsar-receiver. In the current study, the impedance value is set to an ideal 50 Ω. The electric circuit module in COMSOL™ [24] evaluates global variables, voltage, and current as a function of time. The transducer model discussed previously [28] is excited with a Hamming windowed sinusoid signal with amplitude of 160V. The current at the back electrode of the piezoelectric element $\partial^D\Omega_{PZT}$ is given by [24]:

$$\int_{\partial^D\Omega_{PZT}} D \bullet n = Q_0, \frac{dQ_0}{dt} = I_{cir} \tag{11}$$

Hence the voltage on the electrode surface $\partial^D\Omega_{piezo}$ is given by:

$$V_{pz}(t) = V_{source}(t) - I_{cir}R \tag{12}$$

III.E Discretization

A triangular element of maximum size 0.05mm was used for meshing the complete domain $\Omega = \Omega_{SS} \cup \Omega_{Transducer}$. The total number of elements is 256662 with an average growth rate of 1 and an average element quality equal to 0.99. This simulates the defect as a geometric discontinuity which is kept traction free. The maximum element size is determined by the minimum shear wave speed of the material assigned to the computational domain given by [28]:

$$h_{\max} = \frac{c}{f_0 N},\ t = \frac{CFL}{f_0 N} \tag{13}$$

where h_{max} is the maximum element size, c is the shear wave speed in the material, f_0 is the highest frequency required in the spectrum, N is the number of element per wavelength, t is the time step, and CFL (Courant-Freidrich-Levi) number [29] is set equal to 0.2 from the numerical convergence study [28].

III.F Probability of detection formulation

The reflected signal displacement data from the physics based model corresponds to response $\hat{a}$. The true size (here, diameter) of the flaw a is related to response $\hat{a}$ by [30]

$$\hat{a} = \beta_0 + \beta_1 a \tag{14}$$

which is of the linear equation form given by

$$\hat{y} = \beta_0 + \beta_1 x \tag{15}$$

Equation (15) is of the form Ax=b. Using the theory of least square solutions from linear algebra, the estimate for β_j is given by as

$$\begin{bmatrix} \hat{\beta}_0 \\ \hat{\beta}_1 \end{bmatrix} = \left(A^T A\right)^{-1} A^T b \tag{16}$$

If system noise n is added to the equation (15), the modified $\hat{y}$ from equation (15) is then given as

$$\hat{y}_{\text{mod}} = \beta_0 + \beta_1 x + n \tag{17}$$

where system noise n has a normal distribution N (0, τ^2). Using Bessel's correction, τ^2 is given by

$$\tau^2 = \frac{1}{n-1}\sum\left(\hat{y}^2 - \hat{y}_{\text{mod}}{}^2\right) \tag{18}$$

Using the Wald method, given in the standard handbook, MILHDBK-1823A (Appendix G) [30]

$$\text{var}(\hat{y}) = \text{var}(\hat{\beta}_0) + x^2 * \text{var}(\hat{\beta}_1) + 2x * COV(\hat{\beta}_0, \hat{\beta}_1) \tag{19}$$

$$\text{var}(\hat{y}_{\text{mod}}) = \text{var}(\hat{y}) + \tau^2 \tag{20}$$

The decision threshold y_{th} for model data is set to exhibit a conventional nature observed in measurements based POD curves. The detection threshold here is the amplitude of vertical component of displacement field *u* from the model data. The upper and lower 95% confidence bounds are plotted using the probit function. The POD curve is computed by the equation given as,

$$POD = \Theta\left(\frac{\hat{\beta}_0 + \hat{\beta}_1 x - y_{th}}{\sqrt{\mathrm{var}(\hat{y}) + \tau^2}}\right) \tag{21}$$

where Θ is the cumulative distribution function. It should be noted that $\hat{y}$ is the displacement amplitude of the P-wave response from the SDHs computed using the physics based model described previously.

IV. Results and Interpretation

IV.A Model validation and Experimental verification

For the experimental verification, SDHs are machined into a 1018 low carbon steel test blocks at a depth of 25mm as shown in Fig.2. V306 Panametrics 2.25 MHz planar piezoelectric transducer with 12.7 mm nominal element diameter is used for normal incidence contact measurements. For the near field length (N) of 15.6mm, 6dB beam width in the steel at the measured depth of SDHs (1.6N) is 5mm. As the defect size approaches the transducer beam width, the response is not only a function of size of defect, but also a function of reflection ratio and beam width [5] [15]. Hence, the largest flaw size is limited to 3.9mm to reduce the beam width limitation effects. The minimum distance between two adjacent SDHs (22mm) is also greater than the 6dB beam width at a given depth (1.6N) of SDHs.

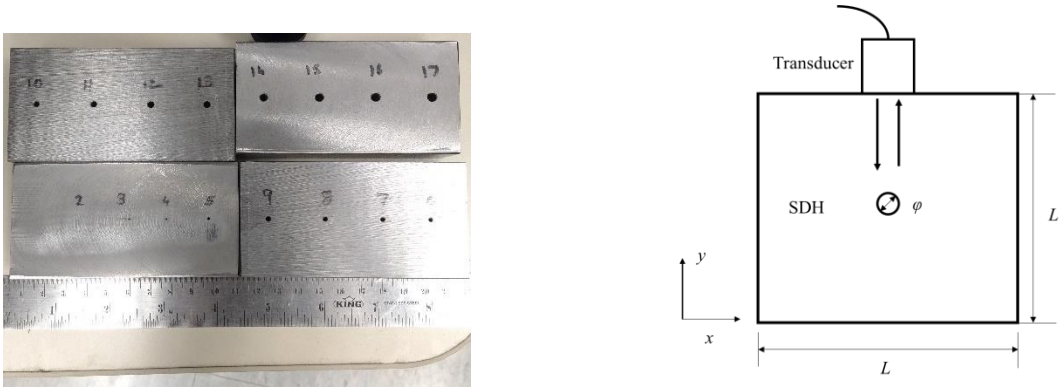

Fig. 2 Side drilled holes with diameter varying from 0.46mm to 3.9 mm in a 1018 low carbon steel block

The Panametrics 5052 pulsar receiver with energy setting at 2, repetition rate at 4, 40 dB gain and damping set at 5 is used with a 1m coax cable and BNC connectors. The measurements acquired using LeCroy HDO 4034 oscilloscope with sampling frequency of 450MHz are averaged 512 times to minimize random electrical noise in the A-scan. Contact measurement for each SDH is repeated 6 times for all 16 SDHs to minimize the variability due to contact pressure. Mean of the six measurements for each SDH response $\left(\bar{x}\right)$ is computed to compare with simulation data. The experimental error for each SDH response is given by $e = \sigma / \sqrt{N}$ where σ is the standard deviation and N is the number of measurements for each SDH. Mean value of experimental error $\left(\bar{e}\right)$ is assigned to the data as shown in Fig. 3(a).

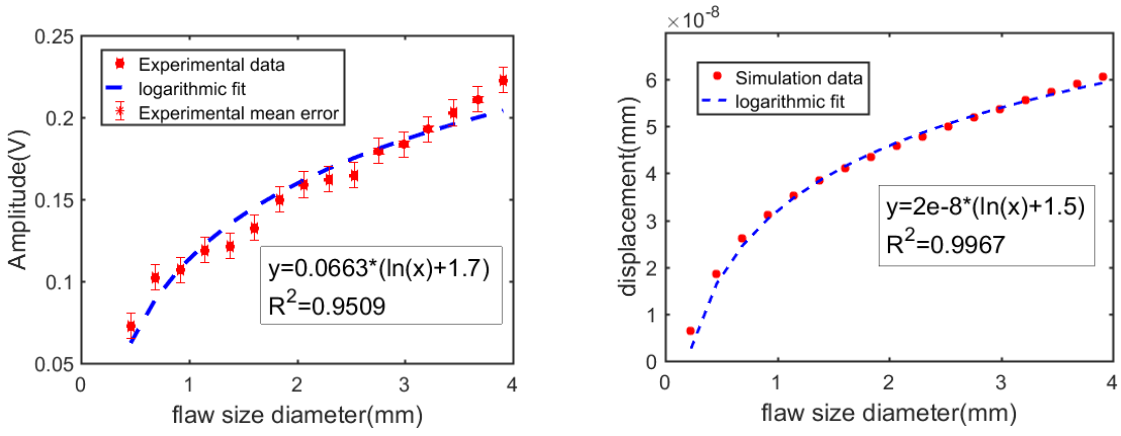

(a) (b)

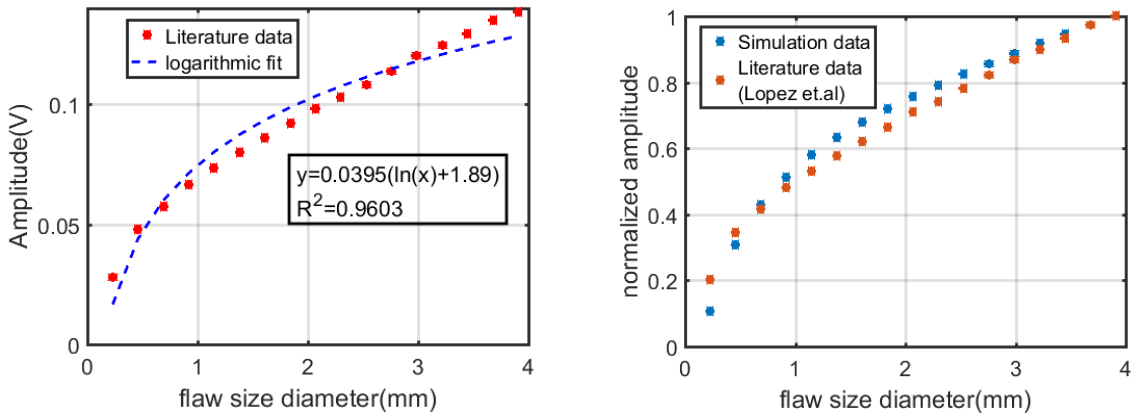

(c) (d)

Fig. 3 P-wave Scattering amplitude for a) Experimental data b) Simulation data c) Literature model data [31] d) Comparison of normalized FE simulation and literature model data

Fig.3(b) shows FE model based P-wave scattering amplitude as a function of SDH diameter. Fig. 3(c) shows scattering amplitude model data for SDH reported by Lopez et al. [31]. The increase in the normalized scattering amplitude as a function of flaw size is in good agreement with literature data as shown in Fig.3(d). For Fig.3(a) through Fig.3(c) scattering amplitude can be fitted logarithmically in the form given by $y=m[ln(x)+c]$. The experimental data shown in Fig.3(a) acquired in terms of voltage amplitude is dependent upon the excitation pulse using the pulsar-receiver circuit. The scattering amplitude from the FE simulation is dependent on the amplitude of the input mechanical displacement to the model. As shown in Table I, this is expressed as the multiplier factor m_i in the fitted equations.

Table I Logarithmic fitting of the data

Data	Equation	m_i	R^2
Experimental data	$y=0.0663(\ln(x)+1.7)$	0.0663	0.95
FE model data	$y=2e\text{-}8(\ln(x)+1.5)$	2e-8	0.99
Literature model data	$y=0.0395(\ln(x)+1.89)$	0.0395	0.96

This effect needs to be compensated to compare model and experimental data. The scattering amplitudes from experiment and models, corrected for the multiplier effect are thus given by

$$y'_{sim} = \frac{y_{sim}}{m_1} = \frac{y_{sim}}{2e-8} \approx \ln(x) + 1.5 \tag{22}$$

$$y'_{\exp} = \frac{y_{\exp}}{m_2} = \frac{y_{\exp}}{0.0663} \approx \ln(x) + 1.7 \tag{23}$$

$$y'_{lit} = \frac{y_{lit}}{m_3} = \frac{y_{lit}}{0.0395} \approx \ln(x) + 1.89 \tag{24}$$

Fig.4 (a-b) shows a good agreement between model and experimental data for 0.4< d/λ<1 using the corrected scattering amplitudes of the SDHs from equation (22) through (24).

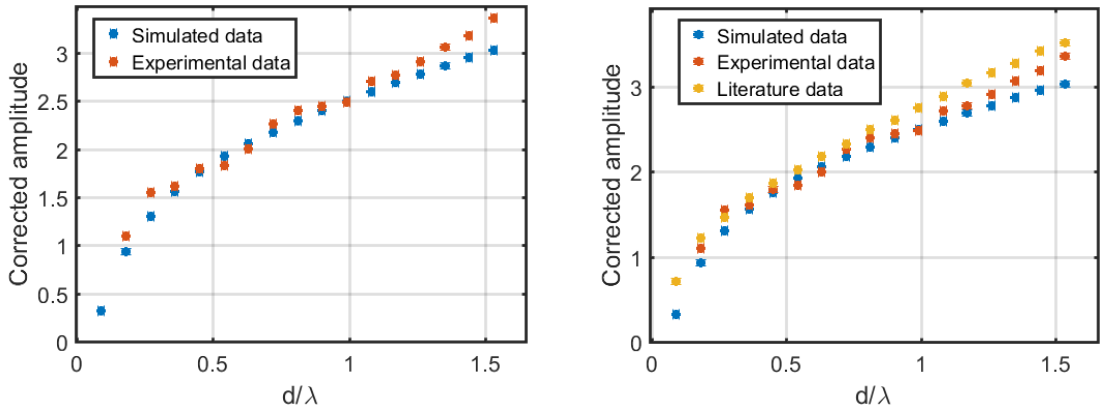

(a) (b)

Fig. 4 (a-b) Comparison of corrected P-wave scattering amplitudes from simulation data, experimental data and previous published model data [31] for SDH

For the d/λ greater than 1, the experimental scattering amplitude shows divergence from the FE model data. The transfer factors m_1 and m_2 from equation (22) and (23) will be used to transform temperature effect from physics based model to the experimental POD.

IV.B Model data for scattering amplitude variation due to temperature dependency of PZT-5A

In this model case, the material coefficients corresponding to a particular temperature are based upon the temperature dependent material coefficient in the literature [25]. The summed temperature effect on all the material coefficients from equation (5) results in the reduction of the scattering amplitude with increase in temperature from 15C to 195C as shown in Fig.5.

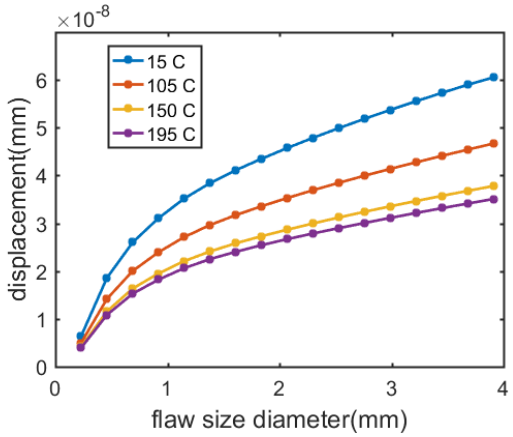

Fig. 5 Displacement versus flaw size (diameter) due to the temperature dependence of material coefficients of PZT-5A

According to the experimental data [25], the magnitudes of s_{11}, s_{13}, s_{33}, s_{44} coefficients reduce whereas d_{33}, d_{31}, ε_{33} ,ε_{11} increase as a function of temperature from 15C to 195C due to the extrinsic and intrinsic contributions in the piezoelectric ceramic[25]. Magnitude change in each of the material coefficients as a function of temperature contributes to the change in total mechanical strain S_i and dielectric displacement D_m as described by equation (3) through (5). This influence of temperature on piezoelectric effect is related to the P-wave scattering amplitude reduction through equation (6) and (10). The logarithmic fitting of the simulated data in the form of equation (14) is shown in Table II where $\hat{a}$ is the simulated reflected echo amplitude from SDH and a is the true size of the SDH**.**

Table II Logarithmic fitting of simulated data

Temperature	Equation	β_1	β_0
15 C	$\hat{a} = 1e-8(2*\ln(a)+3)$	2e-8	3e-8
105 C	$\hat{a} = 1e-8(1*\ln(a)+3)$	1e-8	3e-8
150 C	$\hat{a} = 1e-8(1*\ln(a)+2)$	1e-8	2e-8
195 C	$\hat{a} = 1e-8(1*\ln(a)+2)$	1e-8	2e-8

As the temperature increases from 15C to 105C, β_1 reduces from 50% and β_0 remains unchanged. Increasing temperature of the piezoelectric material from 105C to 150C reduces the value of β_0 by 66% while the value

of β_1 remains unchanged. It should be noted that from 150C to 195C there is no change in the equation used for logarithmically fitting the data.

IV.C Probability of detection (POD) curve with temperature dependency of PZT-5A

Using equations (14) through (21), POD values are calculated and the resulting data is plotted from the physics based model data for different temperatures. The detection threshold Y_{th} is expressed as the amplitude of vertical component of the mechanical displacement field u from the model data. Fig 6 (a) through Fig. 7(b) show POD values for 15C, 105C,150C, and 195C

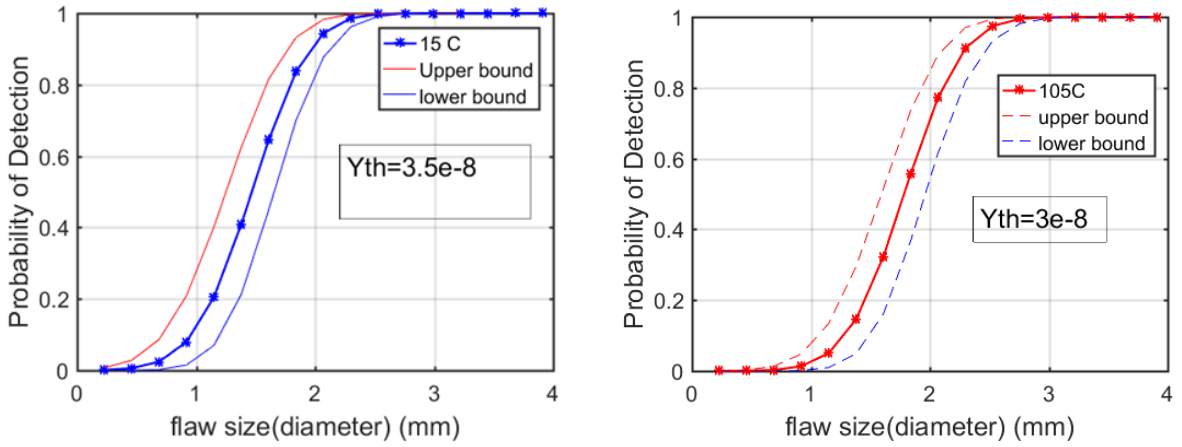

Fig. 6 Probability of detection: (a) 15 C (b) 105 C for the predefined detection threshold Y_{th}

It should be noted that as the temperature is increased, the detection threshold needed to be lowered due to reduction in the scattering amplitude as explained in the previous section. However, the detection threshold is conventionally a system limitation which should be unmodified irrespective of the temperature. Hence, Y_{th} (3.5e-8 mm) at 15C is selected as a fixed threshold for temperatures up to 195C.

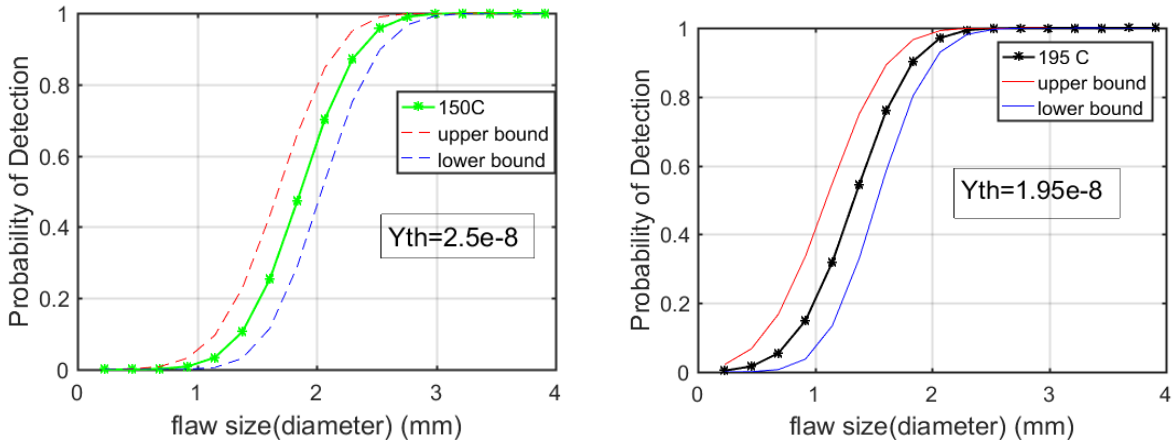

Fig. 7 Probability of detection at: (a) 150 C (b) 195 C for the predefined detection threshold Y_{th}

Fig. 8 shows POD values for temperature increasing from 15C to 195C . It can be seen from Fig. 8 that, increase in the temperature of the PZT-5A introduces a considerable source of variability in the POD for a given flaw size.

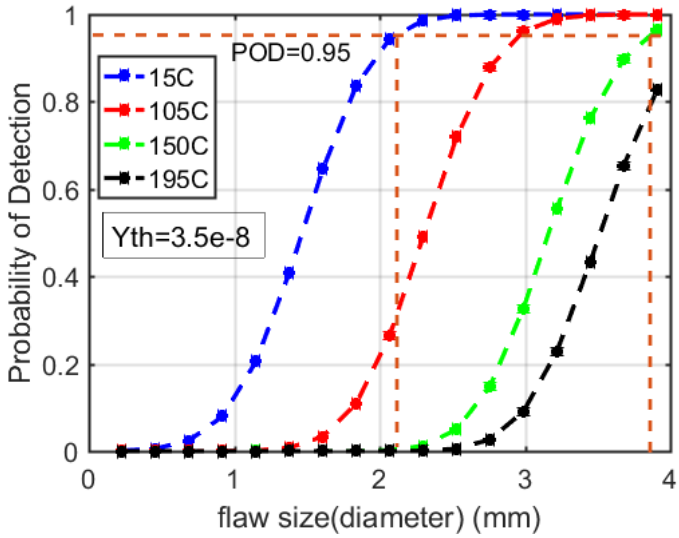

Fig. 8 Effect of temperature dependence of PZT -5A on the POD curve for a fixed threshold (Yth at 15C) (orange dashed line showed flaw size at POD=0.95 from 15C to 195C)

The flaw size corresponding to POD=0.95 increases from 2.1mm (0.81λ) at 15C to more than 1.5 λ at 195C as shown in Fig.8. This shows that detectability of the defects with a probability of 0.95 limits to the flaw size of 1.5 λ at 195C as compared 0.81λ at 15C at 2.25MHz resonance center frequency.

Moreover, for SDHs with a diameter between 0.54λ (1.4mm) and 1.17λ (3mm) in the low carbon steel the POD value varies significantly for 2.25MHz transducer as shown in Fig. 8. For instance, the POD is estimated to reduce by 17% at 195C as compared to 15C for a flaw size 3.9mm (1.5λ) as shown in Fig. 8. For artificial defects such as SDHs of size 1.1λ, a significant 97% reduction in the POD value between 15C and 195C can be seen due to the temperature effect on the piezoelectric material. Table III quantifies the effect of temperature dependency for PZT-5A piezoelectric material properties at 2.25 MHz on the POD values.

Table III Model based data for POD as a function of flaw size for temperature dependence of PZT-5A

SDH (d) (mm)	d/λ	POD (Y_{th}=3.5e-8)			
		15 C	105 C	150 C	195 C
0.23	0.09	0.001	0	0	0
0.46	0.18	0.005	0	0	0
0.69	0.27	0.024	0	0	0
0.92	0.36	0.08	0.0001	0	0
1.15	0.45	0.21	0.001	0	0
1.38	0.54	0.41	0.008	0	0
1.61	0.63	0.64	0.033	0	0
1.84	0.72	0.84	0.11	0	0
2.07	0.81	**0.94**	0.26	0.002	0
2.3	0.9	0.99	0.49	0.012	0
2.53	0.99	1	0.72	0.05	0.006
2.76	1.08	1	0.88	0.15	0.03
2.99	1.17	1	**0.96**	0.33	0.091
3.22	1.26	1	0.99	0.55	0.23
3.45	1.35	1	1	0.76	0.43
3.68	1.44	1	1	0.9	0.65
3.91	1.53	1	1	**0.96**	0.83

IV.D Temperature correction factor *K*

In sections IV.A through IV.C, the material coefficients for PZT-5A are altered based on the experimental data [25] at corresponding temperatures. The effect of the temperature dependent coefficients on the scattering amplitudes and hence the simulation based POD is quantified in Fig.5 and Fig.8 respectively.

In this section, using the simulated data for temperature dependent scattering amplitudes, a correction factor *K* for the temperature effect of PZT-5A is proposed which is calculated as the ratio of the P-wave scattering amplitudes at 15C to the scattering amplitude at the corresponding temperature. The numerical uncertainty in the correction factor is *K*±0.02 with the maximum deviation at SDH of 0.23mm diameter. As shown in Fig. 9(b), the value of K at corresponding temperatures is essentially the magnitude by which the P-wave scattering amplitude needs to be compensated to match the POD at 15C.

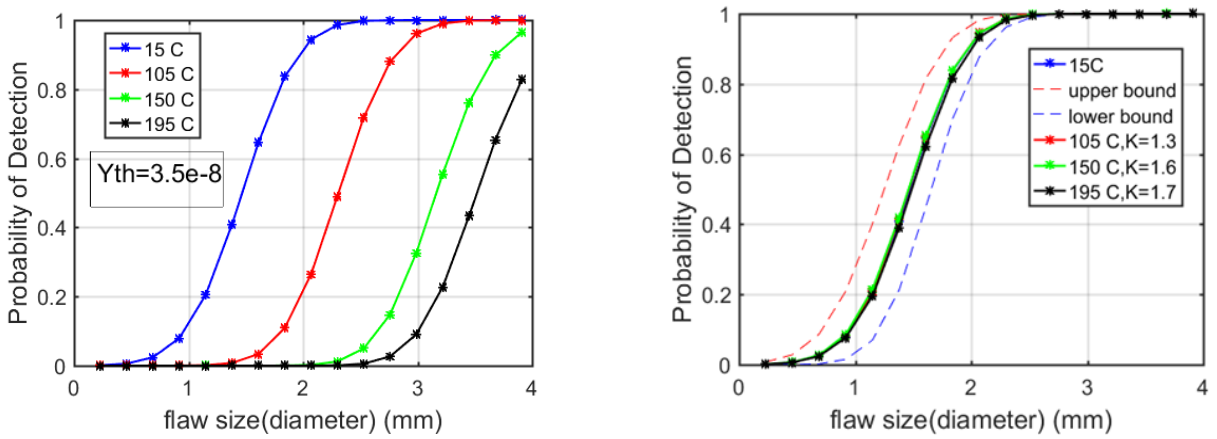

Fig. 9 Model based POD a) Without correction factor b) With PZT-5A temperature correction factor K. (dashed line (red, blue) indicate 95% confidence bounds for POD curve at 15 C

IV.E Estimation of High temperature POD using room temperature experimental data

In order to apply the temperature correction factor *K* from physics based model to the actual experimental data, the detection threshold is set as

$$V_{th} = \frac{Y_{th}}{m_1} * m_2 \approx 0.12V \tag{25}$$

where Y_{th} =3.5e-8 (mm) is detection threshold for the model data at 15C and the transfer factors m_1,m_2 were obtained from equation (22) and (23). Now, using this temperature correction factor *K*, reduction in the

scattering amplitudes of room temperature experimental data is calculated for 105C,150C, and 195C. In this way, Fig. 10 shows the estimation of high temperature (HT) POD using room temperature experimental data, correction factor *K* and transfer factors m_1,and m_2.

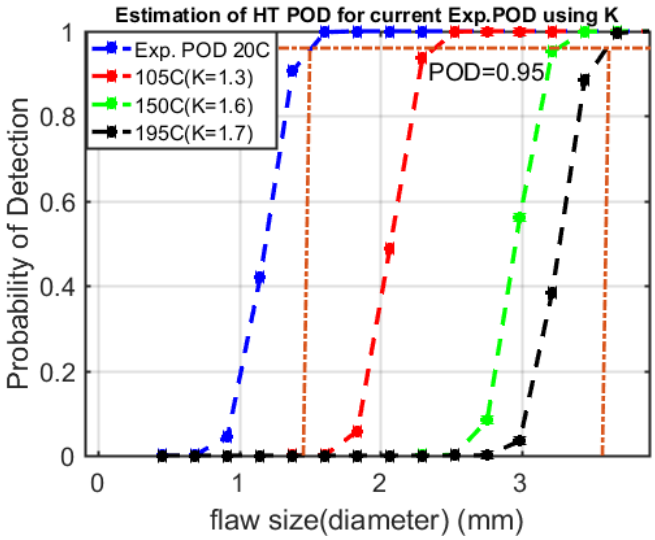

Fig. 10 Estimation of High temperature(HT) POD using room temperature experimental POD (dashed blue line) with temperature correction factor for PZT-5A, obtained from the physics based model

The flaw size corresponding to POD=0.95 increases from 1.49mm (0.58λ) at 15C to 3.58mm (1.41 λ) at 195C as shown by orange dashed line in Fig.10. This shows that detectability of the defects with a probability of 0.95 limits to the flaw size of 1.41 λ at 195C as compared 0.58λ at 15C. In other words, the temperature dependence of PZT-5A reduces the ability of 2.25 MHz transducer to detect smaller defects which otherwise would be possible to detect at 15C with POD=0.95.

V. Conclusion

Current work demonstrated a finite element pulse-echo model for scattering due to a cylindrical side drilled hole (SDH) in a steel specimen. The simulated P-wave scattering amplitude response from SDHs is in good agreement with the experimental and literature data for $0.4<d/\lambda<1$ after correcting for experimental and numerical uncertainties. In the experimental and simulated data, near unity value of coefficient of determination (R^2) indicated that the P-wave scattering amplitude due to SDH can be well represented by a logarithmic fitting and as a function of a SDH diameter. The P-wave scattering amplitude reduces as a

function of temperature due to variation in the piezoelectric material parameters affecting the mechanical strain and electric displacement of the piezoelectric ceramic. This changed the slope and intercept of the logarithmically fitted data. The detection threshold for the simulation based POD needed to be lowered as the temperature increased from 15C to 195C. For a constant threshold value, significant reduction in POD was predicted, particularly in the SDHs with diameter from 1.4 mm (0.54λ) to 3mm (1.17λ). A temperature correction factor is proposed using scattering amplitudes estimated for 15C,105C,150C, and 195C from the physics based model. This correction factor represented the change in the material coefficients of PZT-5A due to temperature dependent intrinsic and extrinsic contributions within the ceramic at a high temperature. Using the transfer factors obtained from experimental and simulated data, a detection threshold is formulated to calculate POD for experimental data at room temperature. Finally, using this experimental data, temperature specific correction factor K and the transfer factors m_1, and m_2, a model based approach has been demonstrated to estimate POD at high temperature using low temperature ultrasonic pulse-echo measurements. The estimated POD data shows that detectability with a probability of 0.95 limits to the flaw size of 1.41 λ at 195C as compared 0.58λ at 15C. In other words, the temperature dependence of PZT-5A reduces the ability of 2.25 MHz transducer to detect smaller defects which otherwise would be possible to detect at 15C with POD=0.95.

Acknowledgement

This work is funded by the U.S. Department of Energy's office of Nuclear Energy under Nuclear Energy University programs (NEUP) and performed at the Centre for NDE at Iowa State University. The authors would like to acknowledge the assistance of Dr. Sabat (Department of Physics, Royal Military College of Canada, Kingston, Ontario K7K 7B4, Canada) [24] who provided the experimental data for PZT-5A (EC-65).

References

[1] OECD "Technology roadmap update for generation IV nuclear energy systems," OECD Nuclear Energy Agency for the Generation IV International Forum (2014). https://www.gen-4.org/gif/upload/docs/application/pdf/2014-03/gif-tru2014.pdf

[2] CEA "4th-generation sodium-cooled fast reactors The ASTRID Technological Demonstrator," Direction de l'énergie nucléaire (nuclear energy division), Centre de Saclay, CEA (2012).

[3] Griffin, J. W., Peters, T. J., Posakony, G. J., Chien, H. T., Bond, L. J., Denslow, K. M., Sheen, S. H. and Raptis, P. "Under-Sodium viewing: a review of ultrasonic imaging technology for liquid metal fast reactors," PNNL-18292, Pacific Northwest National Laboratory, Richland, WA (2009).

[4] Meeker, W. Q. "RB Thompson's contributions to model assisted probability of detection". In *Proc. Review of Progress in Quantitative Nondestructive Evaluation:* Vol. 31, AIP Conference Proceedings # 1430, No. 1, 83-94, AIP Publishing (2012).

[5] Sarkar, P., Meeker, W. Q., Thompson, R. B., Gray, T. A., and Junker, W. "Probability of detection modeling for ultrasonic testing*"* In *Proc. Review of Progress in Quantitative Nondestructive Evaluation*, Vol.17, Plenum press, New York, 2045-2052, Springer US (1998).

[6] Thompson, R. B. "A Unified Approach to The Model-Assisted Determination of Probability of Detection". In D. O. Thompson, & D. E. Chimenti (Eds.), In *AIP Conference Proceedings*, ***975***(1), 1685-1692 (2008).

[7] Thompson, R. Bruce; Brasche, Lisa H.; Forsyth, D.; Lindgren, E.; Swindell, P.; and Winfree, W., "Recent Advances in Model-Assisted Probability of Detection" In *Proc. 4th European-American Workshop on Reliability of NDE* (2009).

[8] Cobb, A. C., Fisher, J., and Michaels, J. E. "Model-assisted probability of detection for ultrasonic structural health monitoring". In *Proc. 4th European-American Workshop on Reliability of NDE* (2009).

[9] Smith, K., Thompson, B., Meeker, B., Gray, T., and Brasche, L. "Model-Assisted Probability of Detection Validation for Immersion Ultrasonic Application". In D. O. Thompson, & D. E. Chimenti (Eds.), In *AIP Conference Proceedings*, Vol. 894, No. 1, 1816-1822 (2007).

[10] Smith, K. D. "POD Transfer Function Approach". In *MAPOD Working Group Meeting*, Vol. 4 (2005).

[11] Aldrin, J. C., Medina, E. A., Lindgren, E. A., Buynak, C. F., and Knopp, J. S. "Protocol for reliability assessment of structural health monitoring systems incorporating model-assisted probability of detection (MAPOD) approach" Air Force Research Lab Wright-Patterson AFB Materials and Manufacturing Directorate (2011).

[12] Jensen, F., Mahaut, S., Calmon, P., and Poidevin, C. "Simulation based POD evaluation of NDI techniques". In *Proc 10th European Conference on Non-destructive Testing* (2010).

[13] Wirdelius, H., and Persson, G. "Simulation based validation of the detection capacity of an ultrasonic inspection procedure" *International Journal of Fatigue*, ***41***, 23-29 (2012).

[14] Pavlovi, M., Takahashi, K., and Müller, C. "Probability of detection as a function of multiple influencing parameters" *Insight-Non-Destructive Testing and Condition Monitoring*, ***54***(11), 606-611 (2012).

[15] Li, M., Meeker, W. Q., and Thompson, R. B. "Physical model-assisted probability of detection of flaws in titanium forgings using ultrasonic nondestructive evaluation" *Technometrics*, ***56***(1), 78-91 (2014).

[16] Subair, S. M., Balasubramaniam, K., Rajagopal, P., Kumar, A., Rao, B. P., and Jayakumar, T., "Finite element simulations to predict probability of detection (PoD) curves for ultrasonic inspection of nuclear components" *Procedia Engineering*, ***86***, 461-468 (2014).

[17] Roy, S., Lonkar, K., Janapati, V., and Chang, F. K., "A novel physics-based temperature compensation model for structural health monitoring using ultrasonic guided waves" *Structural Health Monitoring*, ***13***(3), 321-342 (2014).

[18] Wang, Y., Gao, L., Yuan, S., Qiu, L., and Qing, X. "An adaptive filter–based temperature compensation technique for structural health monitoring" *Journal of Intelligent Material Systems and Structures*, ***25***(17), 2187-2198 (2014).

[19] Salmanpour, M. S., Khodaei, Z. S., and Aliabadi, M. H. "Guided wave temperature correction methods in structural health monitoring" *Journal of Intelligent Material Systems and Structures*, ***28***(5), 604-618 (2017).

[20] Gianneo, A., Carboni, M., Müller, C., and Ronneteg, U. "UPAUT inspection of copper canister: Structural attenuation and POD formulation" *In Review of Progress in QNDE*, Vol. 35, D. E. Chimenti, and L. J. Bond (Eds.), *AIP Conference Proceedings* # 1706, paper 200005, AIP Publishing (2016).

[21] Gianneo, A., Carboni, M., and Giglio, M. “Feasibility study of a multi-parameter probability of detection formulation for a Lamb waves–based structural health monitoring approach to light alloy aeronautical plates” *Structural Health Monitoring*, ***16***(2), pp. 225-249 (2017).

[22] Yusa, N., Chen, W., and Hashizume, H. “Demonstration of probability of detection taking consideration of both the length and the depth of a flaw explicitly” *NDT&E International*, ***81***, 1-8 (2016).

[23] Janapati, V., Kopsaftopoulos, F., Li, F., Lee, S. J., and Chang, F. K., “Damage detection sensitivity characterization of acousto-ultrasound-based structural health monitoring techniques” *Structural Health Monitoring*, ***15***(2), 143-161 (2016).

[24] Comsol Multiphysics, version 5.2. COMSOL AB, Stockholm, Sweden (2016).

[25] Sabat, R. G., Mukherjee, B. K., Ren, W., and Yang, G. “Temperature dependence of the complete material coefficients matrix of soft and hard doped piezoelectric lead zirconate titanate ceramics” *Journal of Applied Physics*, ***101***(6), 06411 (2007).

[26] Baptista, F. G., Budoya, D. E., de Almeida, V. A., and Ulson, J. A. C. “An experimental study on the effect of temperature on piezoelectric sensors for impedance-based structural health monitoring” *Sensors*, ***14***(1), 1208-1227 (2014).

[27] Rose, J.L., Ultrasonic waves in solid media, Cambridge University Press (2004).

[28] Bilgunde, P. N., and Bond, L. J. “A 2D finite element simulation of liquid coupled ultrasonic NDT system.” In *41st Annual Review of Progress in Quantitative Nondestructive Evaluation*, Volume 34 (Vol. 1650), 1543–1552 (2015).

[29] Courant,R., Friedrichs K., and Lewy, H. "Über die partiellen Differenzengleichungen der mathematischen Physik," *Mathematische Annalen*, ***100***(1), 32-74 (1928).

[30] U.S. Department of Defense, MIL-HDBK-1823A Nondestructive Evaluation System Reliability Assessment, Appendix G (2010).

[31] Lopez-Sanchez, A. L., Kim, H. J., Schmerr, L. W., and Sedov, A. “Measurement models and scattering models for predicting the ultrasonic pulse-echo response from side-drilled holes” *Journal of Nondestructive Evaluation*, ***24***(3), 83-96 (2005)